Title: Force-based assessment captures unseen changes in normal and abnormal arm motion

Authors: Ariel B. Thomas[1,2], Erienne V. Olesh[1,2], Amelia Adcock[3,4], and Valeriya Gritsenko[1,2,*]

Affiliations

[1] Department of Human Performance, Division of Physical Therapy, School of Medicine West Virginia University, Morgantown, WV, 26506

[2] Rockefeller Neuroscience Institute, Department of Neuroscience, West Virginia University, Morgantown, WV, 26506

[3] WVU Center for Teleneurology and Telestroke, Morgantown, WV, 26506

[4] Department of Neurology, School of Medicine, West Virginia University, Morgantown, WV, 26506

[*] Valeriya Gritsenko, PO Box 9226, One Medical Center Drive, Morgantown, WV, 26505-9226

Abstract

The way we move changes throughout our lifetime and often we move less as we age. Sometimes this slowdown is due to normal aging, other times the changes are caused by medical issues, such as stroke. The whole repertoire of human motion is enabled by unseen forces applied by our muscles and controlled by our complex nervous system. However, the current standard for assessing human movement in all branches of medicine and sports is based on devices that are blind to those forces. Here we developed a new algorithm to estimate muscle forces from the quantitative observation of motion. Using this force-based assessment, we show that aging causes the movements with dominant and non-dominant arms to be less symmetrical, even approaching the magnitude of interlimb differences caused by stroke. We also show that the force-based assessment provides consistently higher quality measures of individual motor deficits due to stroke compared to traditional motion-based assessment. Our force-based assessment enables a new type of automated measurement of human motion that can be used with current wearable technology for performance assessment and with telemedicine and mobile health initiatives for remote patient monitoring.

Introduction

Movement is a complex interplay between forces generated by our muscles under the control of the central nervous system and the environment. When aging or neurological diseases damage the neuromuscular mechanisms of movement production, this fine interplay is disrupted leading to movement impairment, disability, and inactivity. Stroke is the leading cause of long-term disability in the United States (Centers for Disease Control and Prevention (CDC), 2009) with most stroke survivors experiencing movement deficits that are often accompanied by declining motor function. Some evidence exists that stroke accelerates functional decline due to aging (Dhamoon et al., 2017). Inactivity and aging are two of the highest risk factors for stroke. With age, less than 23% of adults in the United States report exercising enough to meet government guidelines for physical activity (Benjamin et al., 2019). Lack of physical activity increases the risk of stroke, so that up to 90% of it could be attributed to risk factors that relate directly or indirectly to the lack of physical activity (Benjamin et al., 2019). Thus, physical inactivity in elderly and motor deficits after neurological disorders are tightly intertwined. This underlies the need to quantify movement with enough precision that will reveal the underlying mechanisms of functional changes with age and neurological disorders.

The current gold standard in the assessment of movement deficits is based on experienced medical professionals identifying motion abnormalities that are characteristic of specific disorders (Fugl-Meyer et al., 1975; Wolf et al., 2001). Due to the complexity of human body and how gravity and external objects affect its motion, the objective rating of observed motion may not be sufficient for diagnosing movement disorders. It is not always possible to infer from the observation of motion what forces were applied by the muscles to make the arm move, even for a seemingly simple judgement of whether the motion is active or passive. For example, force-based analysis has shown that the elbow and wrist motion of a professional baseball pitcher is more passive compared to the unskilled thrower (Gray et al., 2006; Hirashima et al., 2007). This indicates that the neural motor control system of skilled throwers has adapted to take advantage of the whiplash interaction forces between the shoulder and elbow joints in order to make the throwing movement more efficient and more powerful. This type of force-based analysis may provide valuable insights into the assessment of differences between motion of young and elderly individuals and between healthy motion and that affected by neurological disorders. Therefore, this study aims to provide this insight by quantifying the transformation from muscle forces to movement.

Materials and Methods

Participants

Twenty-two human participants were recruited to perform reaching movements to virtual targets with both arms. The participants were divided into three groups, Control, Stroke, and Age-matched. The Control group (23 ± 0.5 years) included 8 participants without any known neurological or musculoskeletal disorders (data was reported in Olesh et al., 2017). The Stroke group included 8 participants (54 ± 14 years), who have suffered single unilateral ischemic stroke at least three months prior to the experiment. The strokes were diagnosed by neurologists at Ruby Memorial Hospital; the lesion locations were established from medical imaging. Potential participants were excluded if they could not produce visible movement with their shoulder and elbow, or if they were unable to provide written consent to participate. The Age-matched group (52 ± 15 years) included 6 participants without any known neurological or musculoskeletal

disorders, whose age was within the mean ± SD of participants in the Stroke group. All participants were right-hand dominant and reported no unrelated movement disorders or significant injuries to their upper extremities. The study and the consent procedure were approved by the Institutional Review Board of West Virginia University (Protocol # 1311129283). All participants provided written consent before participation.

Table 1. Stroke group information.

ID	Gender	Infarct hemi-sphere	Infarct description and location	Age	Years post stroke	Affected movement duration (s)
1	F	Left	Left middle cerebral artery	51	3	0.7 ± 0.13
2	M	Left	Left caudate lenticular nuclei and external horn of the left ventricle	58	5	0.8 ± 0.14
3	M	Right	Right dorsal pontine-medullary lacunar infarction	67	0.5	0.7 ± 0.17
4	M	Right	Lacunar infarct in posterior right putamen and border of right internal capsule	68	0.25	0.6 ± 0.09
5	M	Right	Right middle cerebral artery	23	11	0.7 ± 0.19
6	M	Right	Right middle cerebral artery	60	6	0.6 ± 0.12
7	M	Right	Right middle cerebral artery, extending posteriorly	53	7	0.5 ± 0.17
8	M	Right	Right lateral medullary infarction with occluded right vertebral artery	51	8	1.8 ± 0.55

Experimental Task

During the experiment, participants reached to virtual targets in a center-out task, as described in Olesh et al. (Olesh et al., 2017). Movements were instructed using a virtual reality (VR) software (Vizard by Wolrdviz) and headset (Oculus Rift), which randomly displayed one of 14 targets, 5 cm in diameter, arranged in the horizontal transverse plane and vertical coronal plane, along with a representation of the participant's arm represented from motion capture (Fig 1). A center target was placed in the VR space so that initial arm posture was at 0◦ shoulder flexion, 90◦ elbow flexion, and a 0◦ wrist flexion. For each participant, the distance from the center target to the peripheral targets was scaled to 30% of arm length (anterior acromial point to the distal tip of the index finger). This distance between the central and peripheral targets was on average 20 cm. Our most impaired participant (S8, Table 1) was unable to reach targets reliably with his left arm that was contralateral to stroked hemisphere. Therefore, the reaching distance for this participant was decreased to 15 cm.

Participants were seated and instructed to reach to targets as quickly and as accurately as possible, while keeping their wrist pronated, fingers extended and adducted, and torso immobile. Each movement began with the participant's hand in the center target (Fig. 1A). A movement was

cued by the changing of the color of center target from green to red and the appearance of one peripheral green target. Upon detection of the tip of the participant's finger tracked with motion capture inside the peripheral target radius, its color changed to red, cueing the participant to return to the central target. After the participant reached the center target, the task reset, peripheral target disappeared, and a new one appeared after a half-a-second delay. Movements to each target location were performed in a randomized order and repeated 15 times with rest breaks after bouts of 70 trials or upon request. Each participant repeated this experiment with both arms in separate sessions.

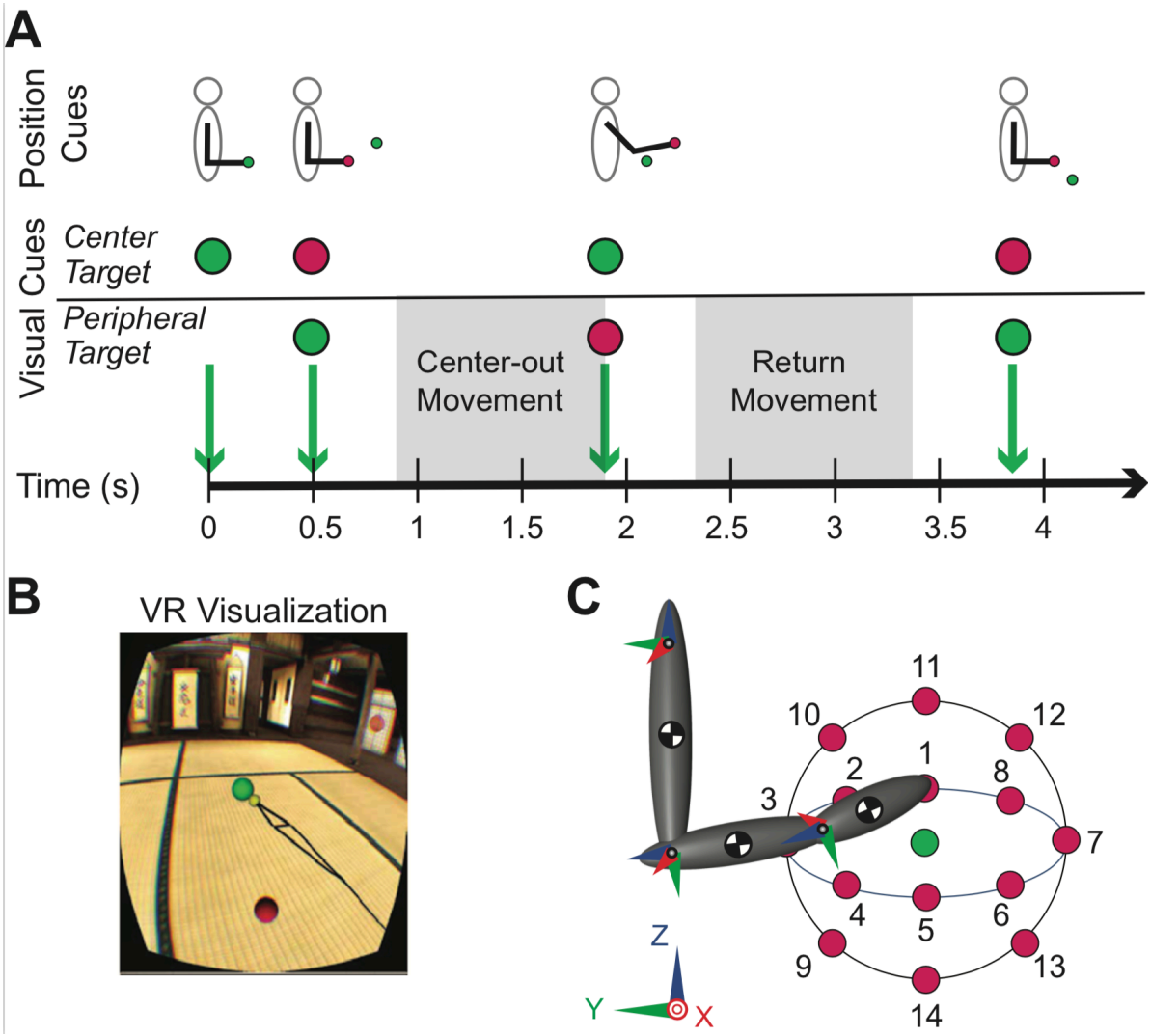

Figure 1. Standardized reaching in virtual reality. A) Trial timeline for each center-out and return reaching movement toward one of 14 peripheral targets. B) Participant's view of the targets in the virtual environment with visual feedback of their limb position (black stick figure indicating hand, forearm, and upper arm) including fingertip (yellow sphere). C) Schematic of the dynamic model of the arm implemented in MATLAB Simulink and used to calculate forces at the shoulder, elbow, and wrist joints. The inertia of major limb segments (humerus, radius/ulna, and hand) were modeled as ellipsoids with the long axes and masses scaled to the lengths of individual participants (Winter, 2009). The checkered circles represent the centers of mass of the segments. Arrows represent the orientations of local and world coordinate systems used for defining joint angles and degrees of freedom. Shoulder, elbow, and wrist flexion/extension degrees of freedom were calculated around X (red) axes. Shoulder abduction/adduction degree of freedom was calculated around Y (green) axis. Shoulder internal/external rotation degree of freedom was calculated around Z (blue) axis. The relative target locations are shown for all movement directions.

Data Processing

Motion capture was recorded during the experiment using an active-marker motion capture system (Impulse by PhaseSpace) and processed in MATLAB (Mathworks Inc.). The light emitting diodes (active markers, LEDs) were placed according to best practice guidelines on anatomical bony landmarks of the arm and trunk (Robertson et al., 2013). Motion capture data were collected at a rate of 480 frames per second, low pass filtered at 10 Hz and interpolated with a cubic spline (maximum interpolated gap: 0.2 s). After the experiment, the onset and offset of each center-out and return movements were identified from the differentiated trajectory of hand marker (velocity) crossing the threshold of 5% of maximal velocity at the beginning and the end of a given movement. These events were verified through visual inspection of the plotted trajectories to correct for unintended motion around the center target and/or corrective movements around the peripheral target. The onset and offset events were used for temporal normalization of kinematic and dynamic profiles prior to averaging. Signals starting 100 ms prior to the onset events were included in the analysis of each movement to capture the full profile of phase-advanced torques.

Inverse Dynamics

Angular kinematics was obtained from motion capture using the coordinate systems illustrated in Fig. 1C. Inverse dynamics simulations using the individually-scaled model shown in Fig. 1C were ran in Simbody (Mathworks) to obtain active muscle torques as described in Olesh et al. (2017). Briefly, joint angles during movement were represented by Euler angles that corresponded to five joint degrees of freedom (DOFs) including 3 shoulder DOFs flexion/extension, abduction/adduction, internal/external rotation, 1 elbow DOF flexion/extension, and 1 wrist DOF flexion/extension. In some participants the medial wrist LED was not reliably tracked due to being obscured frequently from camera view by moving body segments. Therefore, wrist pronation/supination DOF was not reliably detected and, thus, excluded from analysis. Wrist abduction/adduction was found to be minimal during these tasks and was likewise not included in the analysis.

Active muscle torques obtained with inverse simulations were divided into two components, termed postural and dynamic components. The postural torque component captures the portion of muscle torque that supports the limb segments against the force of gravity; it can also be thought of as the postural component of forces produced by muscles. We refer to it as postural forces. The dynamic torque component represents the residual muscle torque related to motion production (Gottlieb et al., 1997; Russo et al., 2014). We refer to it as dynamic forces. This component can also be through of as the muscle force that would produce the same motion without gravity, e.g. in a microgravity environment. As described in Olesh et al. (2017), to obtain the dynamic torque components we ran the inverse dynamics simulations with gravity of the physics engine set to zero. To obtain the postural component, the dynamic torque component was subtracted from the overall active muscle torque obtained from simulations with standard gravity for each DOF.

Statistical Analysis

Angular kinematic and torque signals were normalized in time, resampled to 1000 samples, and averaged. Inter-trial variability was calculated as the standard deviation across repetitions of individual movements toward the same target and averaged over the normalized trajectory samples

(n=15). The individual normalized trajectories were averaged to create a mean signal for each center-out and return movement toward each target for each participant.

The symmetricity between movement of right and left limbs was calculated using the interlimb shared variance metric. To obtain this metric, the coefficient of determination (R^2) was calculated between normalized mean trajectories for corresponding signals from the right and left limbs of the same participant. These values were then averaged across movement for each DOF for each participant. The resulting metric ranged between 0 (low symmetricity or high asymmetricity) and 1 (high symmetricity or low asymmetricity).

To test the null hypotheses that the movements of participants in different groups were equally symmetrical, we applied repeated measures analysis of variance (ANOVA) to interlimb shared variance metric for each signal type, i.e. angular kinematics (Table S1), muscle forces (Table S2), postural forces (Table S3), and dynamic forces (Table S4). All ANOVAs were structured the same way with a single between-subject factor Group with 3 levels (Control, Age-Matched, and Stroke) and two within-subject factors Direction with 28 levels (14 center-out movements to peripheral targets and 14 return movements numbered as in Fig. 1C) and DOF with 5 levels (3 shoulder DOFs flexion/extension, abduction/adduction, internal/external rotation, 1 elbow DOF flexion/extension, and 1 wrist DOF flexion/extension). The p-values with Greenhouse-Geisser adjustment for sphericity (Geisser and Greenhouse, 1958) were used to determine significance.

Results

The reaching movements produced by participants with their right and left limbs were highly symmetrical in Control group, somewhat less symmetrical in Age-matched group, and the least symmetrical in Stroke group (Table 2, Group effect; Fig. 2). The progressively less symmetrical movements across groups were observed for all movement directions (Table 2, interaction). Post-hoc analysis found no significant differences in angular kinematics between Control and Age-matched group across all DOFs and movement directions. Across movement directions, the angular kinematics of the wrist was less symmetrical in Stroke group compared to Age-matched group ($p = 0.02$) and to the Control group ($p = 0.04$), and the angular kinematics of the elbow was less symmetrical in Stroke group compared Control group ($p = 0.02$).

Across all DOFs, the angular kinematics was less symmetrical in Stroke than in Age-matched group for center-out movements ($p_7 = 0.01$, $p_{10} = 0.01$, $p_{11} = 0.03$, $p_{14} = 0.01$) and return movements ($p_8 = 0.01$, $p_{13} < 0.01$). The angular kinematics was less symmetrical in Stroke than in Control group for a single center-out movement ($p_7 = 0.02$) and return movements ($p_2 = 0.01$, $p_{13} < 0.01$).

Table 2: Repeated measures ANOVA on angular kinematics

Factors	**SumSq**	**DF**	**MeanSq**	**F**	***p***
Group	60.01	139	0.43	8.89	< 0.01
Within factors	15.62	278	0.06	1.16	0.28
Group * within factors interaction	114.78		0.05	1.00	0.50

SumSq stands for the sum of squares; DF stands for degrees of freedom; MeanSq stands for mean squared error.

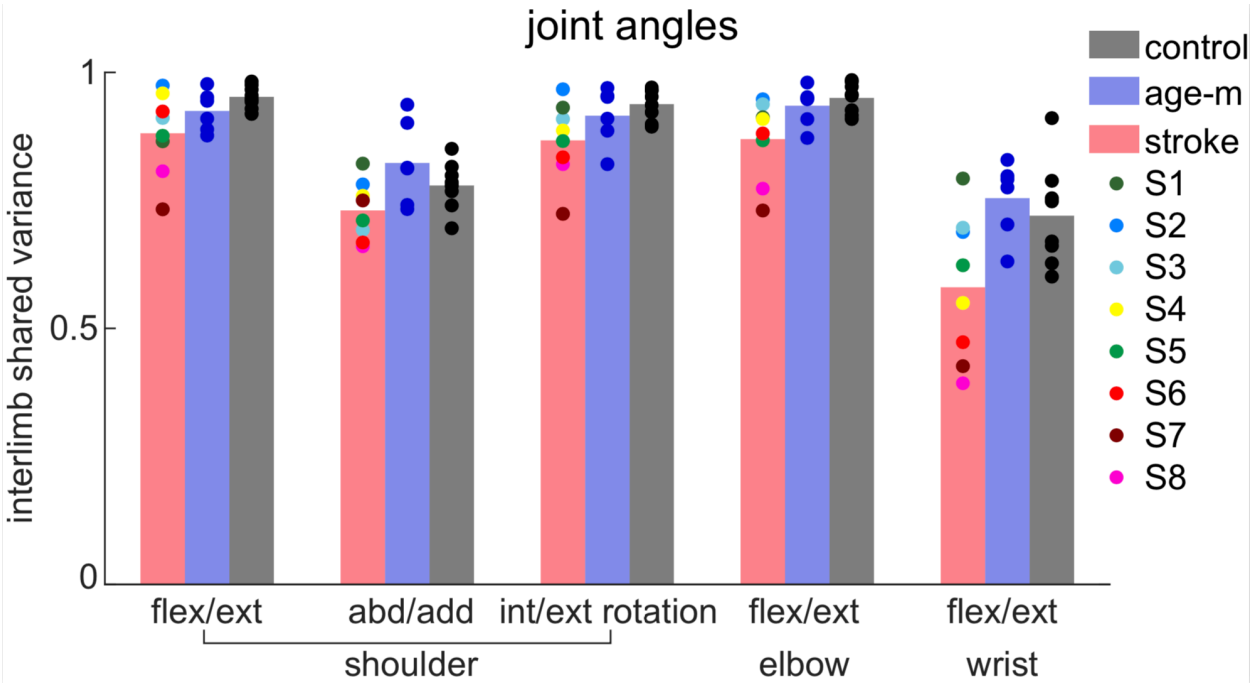

Figure 2. Asymmetricity based on joint angles. Bars show mean interlimb shared variance per group (age-m indicates Age-matched group); symbols show values for individual participants. Joint angle profiles are more similar between limbs for shoulder flexion/extension and internal/external (int/ext) rotation and for elbow flexion/extension. They are less similar between limbs for shoulder abduction/adduction (abd/add) and wrist flexion/extension.

The right and left movements appeared much less symmetrical when observed through active muscle torques than through joint angles (Fig. 3). This metric was also more variable across participants in all groups compared to the metric based on joint angles (Fig. 2). Across movement directions, post-hoc analysis found no significant differences in muscle torques per DOF between Control and Age-matched group, nor between Stroke and Age-matched group (Table 3). The muscle torques were less symmetrical in Stroke than in Control group at the shoulder joint for internal/external rotation DOF ($p < 0.01$), at the elbow joint ($p < 0.01$), and at the wrist joint ($p = 0.01$). Across all joints, the muscle torques were less symmetrical in Age-matched than in Control group for a single center-out movement ($p_2 < 0.01$). The muscle torques were less symmetrical in Stroke than in Age-matched group for the same and one other center-out movement ($p_2 = 0.04$, $p_8 = 0.01$), and they were less symmetrical in Stroke than in Control group for a single return movement ($p_{13} = 0.04$).

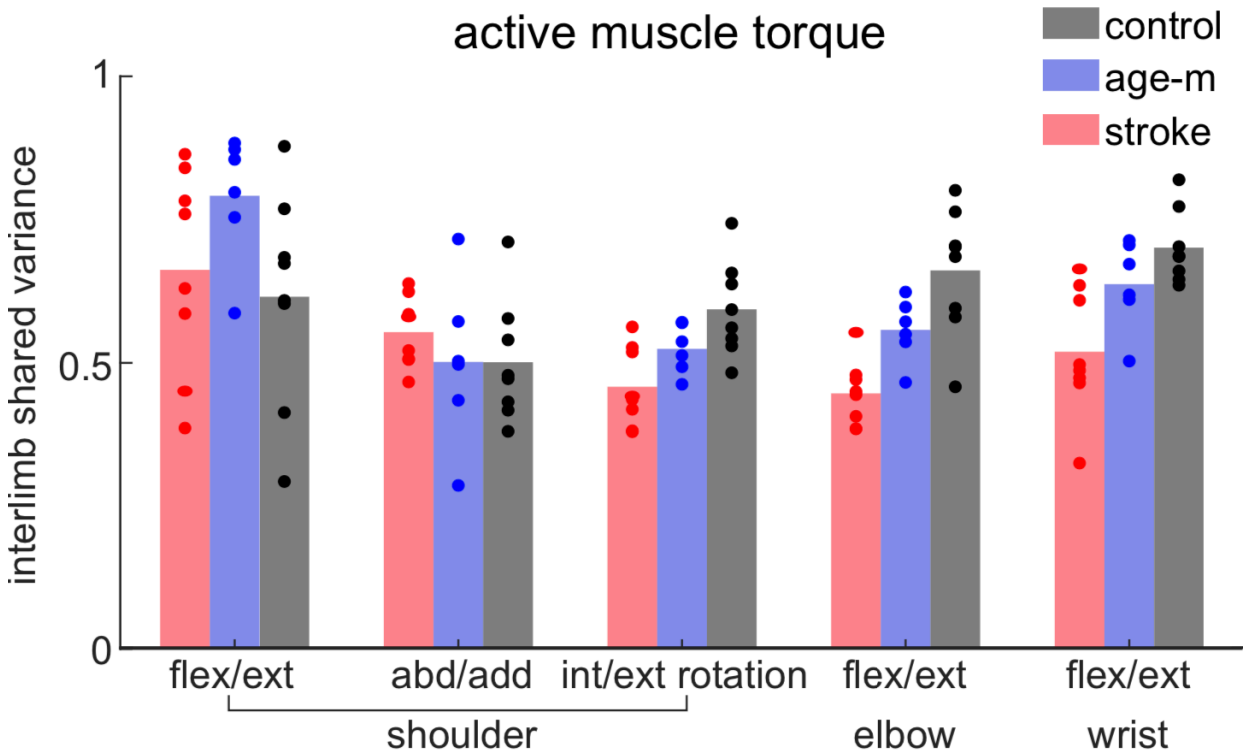

Figure 3. Asymmetricity based on active muscle torque. Bars show mean interlimb shared variance per group (age-m indicates Age-matched group); symbols show values for individual participants. Between limbs, the active muscle torque profiles were less symmetrical than the joint angle profiles across all DOFs and joints.

Table 3: Repeated measures ANOVA on active muscle torque

Factors	SumSq	DF	MeanSq	F	*p*
Group	68.36	139	0.49	5.57	< 0.01
Within factors	33.41	278	0.12	1.36	0.13
Group * within factors interaction	208.72		0.09	1	0.5

SumSq stands for the sum of squares; DF stands for degrees of freedom; MeanSq stands for mean squared error.

Forces exerted by muscles during these movements, muscle torques, were separated into two broad components, postural and dynamic forces (see Methods). We classified postural forces as those needed to overcome gravity, which vary throughout movement as the orientation of limb segments relative to the gravity vector changes. The dynamic forces are those responsible for producing the movement in the absence of gravity and can be thought of as the forces produced by astronauts making the same movement in a microgravity environment.

As with kinematics, we found that the postural forces were less similar between corresponding left and right movements in participants from Age-matched or Stroke groups compared to young control participants (Fig. 4; Table 4). However, the movements appeared more symmetrical when observed through postural forces compared to overall muscle forces (Fig. 3). Interestingly, some of the inter-subject variability observed in the muscle-force metric is preserved in the postural-force metric, particularly in the Stroke group. In contrast, a significant part of inter-subject variability observed in the muscle-force metric goes away in the postural-force metric, particularly in the Control group. Across movement directions, post-hoc analysis found no

significant differences in postural forces per DOF between groups. Across all joints, no significant differences in postural forces per movement direction were found between Control and Age-matched group. The postural forces were less symmetrical in Stroke than in Age-matched group for center-out movements ($p_3 = 0.03$, $p_5 = 0.02$). The postural forces were less symmetrical in Stroke than in Control group for the same center-out movements ($p_3 = 0.02$, $p_5 = 0.04$) and a return to center movement ($p_1 = 0.02$).

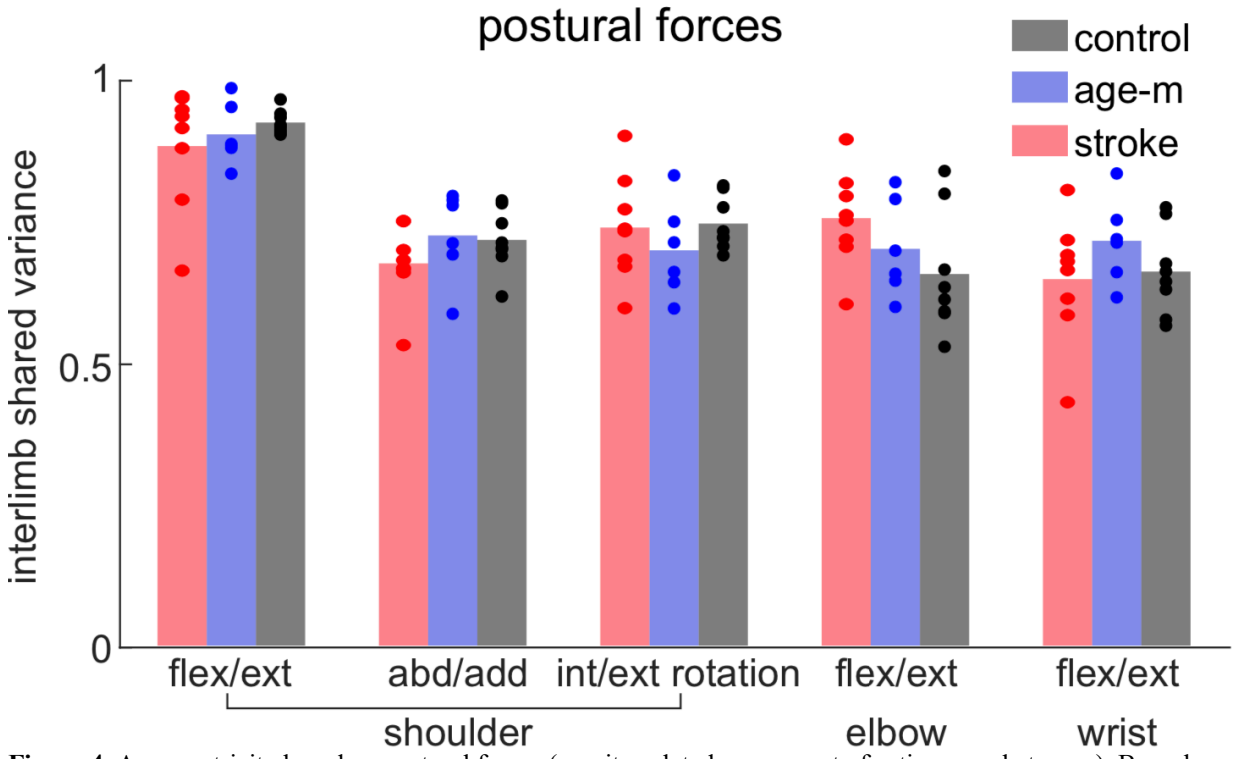

Figure 4. Asymmetricity based on postural forces (gravity-related component of active muscle torque). Bars show mean interlimb shared variance per group (age-m indicates Age-matched group); symbols show values for individual participants. Between limbs, the postural force profiles are more symmetrical than overall muscle torque profiles across all DOFs and joints, and less symmetrical than joint angle profiles for int/ext rotation of the shoulder and flex/ext of the elbow. Additionally, the variability between subjects in the interlimb shared variance based on postural forces is larger than that based on kinematics or dynamic forces.

Table 4: Repeated measures ANOVA on postural forces

Factors	**SumSq**	**DF**	**MeanSq**	**F**	***p***
Group	52.46	139	0.38	4.68	< 0.01
Within factors	29.67	278	0.11	1.32	0.14
Group * within factors interaction	190.63		0.08	1	0.5

SumSq stands for the sum of squares; DF stands for degrees of freedom; MeanSq stands for mean squared error.

The differences between groups were the largest and most consistent when the dynamic forces were analyzed (Fig. 5). The movements were progressively less symmetrical between limbs from Control to Age-matched to Stroke groups across all joints and movement directions (Table 5). In the Age-matched group, the most asymmetrical movements relative to Control group were outward away from the body ($p_5 = 0.05$, $p_7 = 0.01$, $p_8 < 0.01$), downward toward the body ($p_9 = 0.03$, p-value subscript indicates target number in Fig. 1C), and movement up ($p_{11} < 0.01$). In the

Stroke group, the most asymmetrical movements relative to Control group were the same outward movements as in Age-matched group ($p_5 = 0.01$, $p_6 = 0.04$, $p_7 = 0.03$, $p_8 < 0.01$) plus some return to center movements ($p_2 < 0.01$, $p_6 = 0.04$, $p_{13} = 0.01$) and the movement up ($p_{11} < 0.01$). Note that motion asymmetry in Stroke group include both age-related and stroke-related differences between forces produced by left and right limbs. Both kinematic and dynamic data has shown that with age movements produced by dominant and non-dominant limbs differ more. Moreover, the age-related differences in forces between limbs can be as great as those caused by stroke.

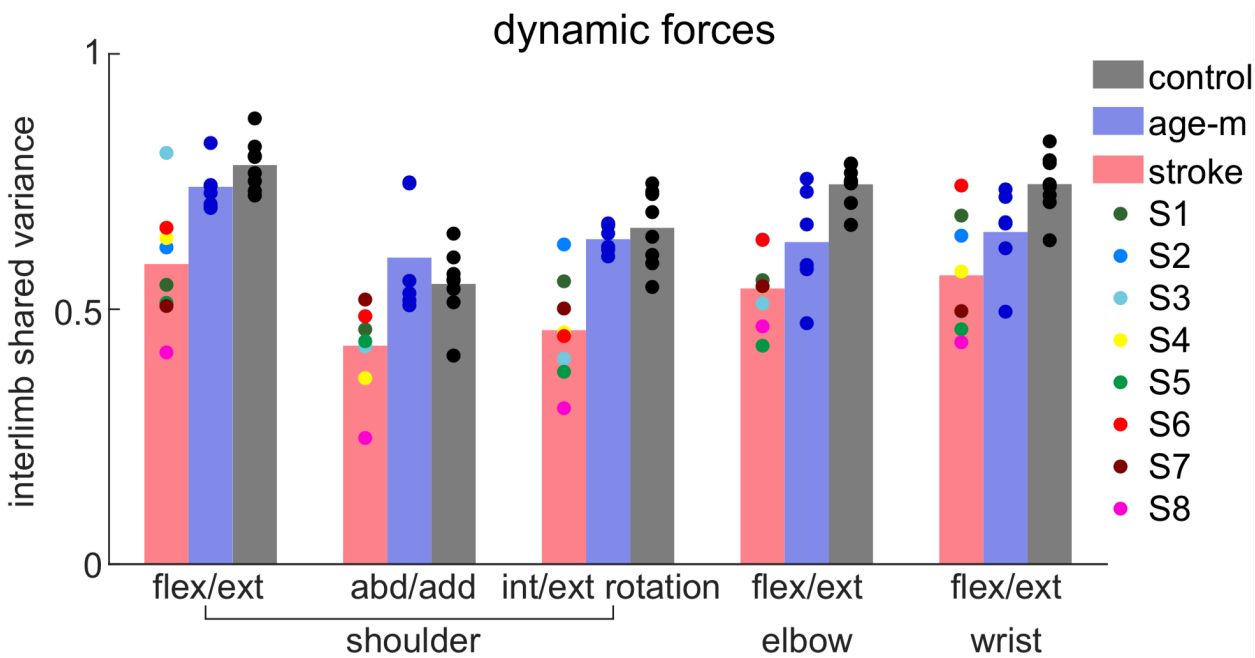

Figure 5. Asymmetricity based on dynamic forces (motion component of active muscle torque). Bars show mean interlimb shared variance per group (age-m indicates Age-matched group); symbols show values for individual participants. Interlimb shared variance for dynamic forces per joint and degree of freedom averaged across movement directions. Between limbs, the dynamic force profiles are generally less similar than the joint angle profiles across all joints.

Table 5: Repeated measures ANOVA on dynamic forces.

Factors	SumSq	DF	MeanSq	F	p
Group	66.72	139	0.48	6.76	< 0.01
Within factors	23.35	278	0.08	1.18	0.25
Group * within factors interaction	167.72		0.07	1	0.5

SumSq stands for the sum of squares; DF stands for degrees of freedom; MeanSq stands for mean squared error.

We also found that comparing dynamic forces produced by each limb resulted in a more sensitive measure of the participant's motor deficits then comparing motion itself, such as joint angles of left and right limbs. Most of the participants in the Stroke group had mild hemiparesis, so that motion with their less-affected ipsilesional arm and more-affected contralesional arm were largely symmetrical. This was reflected in high interlimb shared variance between the joint angle profiles of each limb (Fig. 6A, joint angles). In contrast, the shared variance between the dynamic

torque profiles of the two limbs was much lower in the same participants (Fig. 6B, dynamic forces), indicating a higher degree of motor deficit than what was observed from kinematics. To investigate this difference across multiple movement directions, we calculated the effect size of motor deficit measures based on angles and forces using the following formula: $(1 - R^2_{stroke})/SD(R^2)$, where R^2_{stroke} is the interlimb shared variance of individual participants from the Stroke group and $SD(R^2)$ is the pooled standard deviation of interlimb shared variance across participants from the Age-matched and Stroke groups. We found that across most tested movement directions the effect size of the force-based measure was larger than the effect size of the motion-based measure for most participants (Fig. 6B, magenta lines). This suggests that the sensitivity of the assessment of motor deficits due to stroke can be increased by estimating muscle forces produced during arm motion.

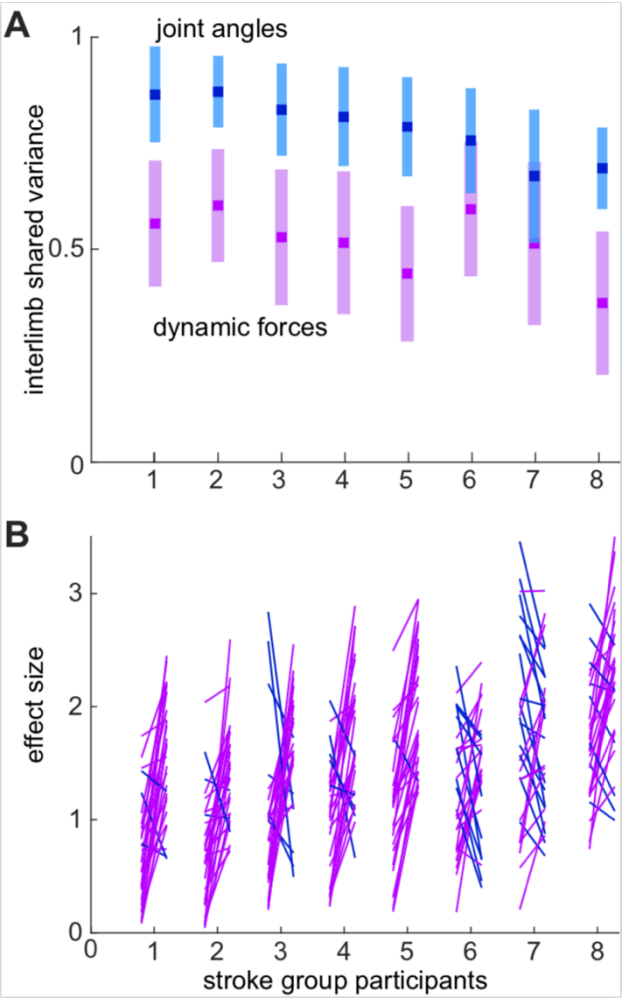

Figure 6. Quantifying movement deficits after stroke using muscle forces is better than that using joint angles. A. Interlimb shared variance for joint angles and dynamic forces averaged across movement directions. The central tendencies of data per subject are shown as means (dark boxes) with standard deviation (light bars). The values for interlimb shared variance for dynamic forces are in the middle of the 0 to 1 range, while those for joint angles are closer to the upper limit of the range for multiple participants, indicating a tendency for saturation. B. Effect size calculated from shared variance between limbs. The lines for each movement direction start on the left of participant's ID at the value for the effect size based on joint angle. The lines end on the right of participant's ID at the value of the effect size based on dynamic forces. The upward slopes (magenta) show larger force-based than angle-based effect sizes for a given movement direction; the downward slopes (blue) show the opposite differences in effect sizes. Across most tested movement directions, the force-based effect sizes were larger than the angle-based effect sizes in most participants.

Discussion

Here we report that as we age the forces produced by our neuromuscular system to make movements with dominant and non-dominant limbs become less symmetrical. This age-related change in how we make movements presents a challenge for the assessment of motor deficits in elderly individuals who have suffered a stroke. The problem is to distinguish between age-related and stroke-related changes in movements in individuals whose pre-stroke state is not known. We propose a possible solution to this problem, which is to assess movement deficits in terms of muscle forces rather than the traditional assessment based on movement kinematics.

We found that force-based measures were more sensitive than motion-based measures to subtle interlimb differences in how the complex reaching movements in different directions were produced by individuals. These findings may provide the context for distinguishing movement changes due to healthy aging from movement deficits due to neurological disorders. Furthermore, the force-based measures are sensitive to individual deficits in movements after a stroke. A force-based assessment developed based on this method could be helpful in tailoring physical therapy and other rehabilitation programs to the individual, especially in patients who have less "observable" deficits as those classified as asymptomatic via traditional motion-based assessments. Technology has advanced to the point where low-cost commercial devices that observe our movement in combination with sophisticated algorithms are becoming widely available for home use. Our study has shown that estimating muscle forces that drive motion can enable a new type of automated assessment of human motor function. This approach can be potentially useful as part of telemedicine and mobile health initiatives, where the patient's health needs to be monitored remotely. Lastly, the analysis of forces that produce movement could also provide unique insight into the underlying mechanisms of neural and musculoskeletal interactions that will inform future therapies.

References

Benjamin EJ, **Muntner P**, **Alonso A**, **Bittencourt MS**, **Callaway CW**, **Carson AP**, **Chamberlain AM**, **Chang AR**, **Cheng S**, **Das SR**, **Delling FN**, **Djousse L**, **Elkind MSV**, **Ferguson JF**, **Fornage M**, **Jordan LC**, **Khan SS**, **Kissela BM**, **Knutson KL**, **Kwan TW**, **Lackland DT**, **Lewis TT**, **Lichtman JH**, **Longenecker CT**, **Loop MS**, **Lutsey PL**, **Martin SS**, **Matsushita K**, **Moran AE**, **Mussolino ME**, **O'Flaherty M**, **Pandey A**, **Perak AM**, **Rosamond WD**, **Roth GA**, **Sampson UKA**, **Satou GM**, **Schroeder EB**, **Shah SH**, **Spartano NL**, **Stokes A**, **Tirschwell DL**, **Tsao CW**, **Turakhia MP**, **VanWagner LB**, **Wilkins JT**, **Wong SS**, **Virani SS**, **American Heart Association Council on Epidemiology and Prevention Statistics Committee and Stroke Statistics Subcommittee**. Heart Disease and Stroke Statistics-2019 Update: A Report From the American Heart Association. *Circulation* 139: e56–e66, 2019.

Centers for Disease Control and Prevention (CDC). Prevalence and most common causes of disability among adults--United States, 2005. [Online]. *MMWR Morb Mortal Wkly Rep* 58: 421–426, 2009. https://www.cdc.gov/mmwr/preview/mmwrhtml/mm5816a2.htm.

Dhamoon MS, **Longstreth WT**, **Bartz TM**, **Kaplan RC**, **Elkind MSV**. Disability Trajectories Before and After Stroke and Myocardial Infarction: The Cardiovascular Health Study. *JAMA Neurol* 74: 1439–1445, 2017.

Fugl-Meyer AR, **Jaasko L**, **Leyman I**, **Olsson S**, **Steglind S**. The post-stroke hemiplegic patient: a method for evaluation of physical performance. *Scand J Rehabil Med* 7: 13–31, 1975.

Geisser S, **Greenhouse SW**. An Extension of Box's Results on the Use of the Distribution in Multivariate Analysis. *The Annals of Mathematical Statistics* 29: 885–891, 1958.

Gottlieb GL, **Song Q**, **Almeida GL**, **Hong DA**, **Corcos D**. Directional control of planar human arm movement. *J Neurophysiol* 78: 2985–2998, 1997.

Gray S, **Watts S**, **Debicki D**, **Hore J**. Comparison of kinematics in skilled and unskilled arms of the same recreational baseball players. *Journal of sports sciences* 24: 1183–1194, 2006.

Hirashima M, **Kudo K**, **Watarai K**, **Ohtsuki T**. Control of 3D limb dynamics in unconstrained overarm throws of different speeds performed by skilled baseball players. *J Neurophysiol* 97: 680–691, 2007.

Olesh EV, **Pollard BS**, **Gritsenko V**. Gravitational and Dynamic Components of Muscle Torque Underlie Tonic and Phasic Muscle Activity during Goal-Directed Reaching. *Front Hum Neurosci* 11: 1–12, 2017.

Robertson G, **Caldwell G**, **Hamill J**, **Kamen G**, **Whittlesey S**. *Research Methods in Biomechanics, 2E*. Human Kinetics, 2013.

Russo M, **D'Andola M**, **Portone A**, **Lacquaniti F**, **d'Avella A**. Dimensionality of joint torques and muscle patterns for reaching. *Front Comput Neurosci* 8: 24, 2014.

Winter DA. *Biomechanics and Motor Control of Human Movement*. 4 ed. Hoboken, New Jersey: John Wiley & Sons, 2009.

Wolf SL, **Catlin PA**, **Ellis M**, **Archer AL**, **Morgan B**, **Piacentino A**. Assessing Wolf motor function test as outcome measure for research in patients after stroke. *Stroke* 32: 1635–1639, 2001.

Acknowledgments

We thank the study participants for generously giving their time, and M. Powers for her assistance with participant recruitment and the general support of the study; we acknowledge the technical support expertly provided by B. Pollard; we are thankful for insightful and critical comments of S. Yakovenko.

Funding

The study was supported by NIH/NIGMS U54GM104942, T32GM081741, T32AG052375, P20GM109098, and P30GM103503.